Stem-FIT and Soil-FIT: Integrated Plant and Soil Nitrogen-Hormone Sensing with Machine Learning-based Forecasting for Next-Generation Precision Agriculture

Nafize I. Hossain
The University of Texas at Tyler
Mohammad Solaiman
The University of Texas at Tyler
Shawana Tabassum
stabassum@uttyler.edu

The University of Texas at Tyler

Article

Keywords: Multiplexed sensors, Plant sap analysis, Soil nutrient monitoring, Phytohormones, Machine Learning, Long short-term memory (LSTM) prediction, Precision agriculture, Stress resilience

Posted Date: November 19th, 2025

DOI: https://doi.org/10.21203/rs.3.rs-7933154/v1

Additional Declarations: No competing interests reported.

Stem-FIT and Soil-FIT: Integrated Plant and Soil Nitrogen-Hormone Sensing with Machine Learning-based Forecasting for Next-Generation Precision Agriculture

Nafize I. Hossain[1,2+], Mohammad Solaiman[1,3+], and Shawana Tabassum[1*]

[1]Department of Electrical and Computer Engineering, The University of Texas at Tyler, Tyler, TX, USA

[2]Department of Electrical and Computer Engineering, Tufts University, Medford, MA, USA

[3]Department of Electrical and Computer Engineering, The University of New Mexico, Albuquerque, NM, USA

+These authors contributed equally

*Corresponding author: stabassum@uttyler.edu

Abstract

Inefficient fertilizer application in agriculture leads to reduced crop productivity, nutrient losses, and reduced crop resilience, highlighting the urgent need for real-time monitoring of plant–soil nutrient dynamics. This research aims to develop and validate a multiplexed sensing platform for simultaneous, in-situ measurement of key soil nutrients (Soil-FIT) and plant phytohormones (Stem-FIT) involved in nitrogen signaling and stress regulation. The proposed sensor suite integrates three 3D-printed modules for continuous monitoring of nitrate, ammonium, and pH in both soil and plant sap, along with salicylic acid (SA), indole-3-acetic acid (IAA), methyl jasmonate (MeJA), and ethylene (ET) in plant sap. The sensors, functionalized with non-enzymatic electrode coatings, were deployed in bell pepper plants grown under four treatment combinations of irrigation (full vs. deficit) and nitrogen application (medium vs. high). Data were collected every three hours over the growing period and analyzed using a long short-term memory (LSTM) model for short-term prediction of nutrient and hormone fluctuations. The sensors exhibited high sensitivity and stability, achieving detection limits of 0.218 μM for IAA, 1.07 μM for MeJA, 1.315 μM for SA, 1.08 ppm for nitrate, 1.017 ppm for ammonium, 0.29 ppm for ethylene, and 0.01 pH. The LSTM model demonstrated strong predictive capability (R^2 = up to 0.86), accurately forecasting short-term variations in plant and soil nutrient–hormone profiles. These findings demonstrate that coupling real-time, multiplexed sensing with machine learning enables early detection and prediction of crop stress, supporting precision nitrogen management and advancing sustainable agricultural practices.

Keywords

Multiplexed sensors, Plant sap analysis, Soil nutrient monitoring, Phytohormones, Machine Learning, Long short-term memory (LSTM) prediction, Precision agriculture, Stress resilience

1. Introduction

Agriculture provides food, fiber, and fodder, and thus plays a critical role in the economic development of many nations[1,2]. Despite this, around 820 million people globally suffer from malnutrition, and with the global population expected to grow by 34% by 2050, food scarcity is likely to worsen[2]. Enhancing agricultural productivity is essential to combat global hunger and poverty[3]. Farmers often over-apply or under-apply fertilizers in an attempt to maximize crop yields[4], which can lead to reduced productivity and economic losses. There are two primary classes of minerals essential for plant growth: macronutrients and micronutrients. Key macronutrients include nitrogen (N), potassium (K), and phosphorus (P), while iron (Fe), zinc (Zn), manganese (Mn), and copper (Cu) are some of the important micronutrients[5]. Among these, nitrogen (N) is the most critical nutrient for plant productivity, as it serves as a fundamental component of amino acids, chlorophyll, and nucleic acids. N deficiency severely impairs photosynthesis, reduces leaf area and chlorophyll content, and restricts shoot and root growth, ultimately leading to diminished biomass accumulation and yield potential[6]. In addition, drought conditions significantly limit nitrate uptake and assimilation by reducing soil moisture, root hydraulic conductivity, and nitrate transporter activity, leading to nutrient imbalances and exacerbated yield losses under water

stress[7,8]. Conversely, excessive use of N, P, and K fertilizers can degrade soil quality and water resources, emphasizing the need for precise and sustainable fertilizer management practices[9]. Research shows that plants utilize only a small portion of applied nutrients, with most N lost through leaching, runoff, or conversion to greenhouse gases. On average, 12.5% of nitrate[10] and 0.75-1.95% of phosphate[11] are lost annually via leaching and runoff due to their high solubility and mobility in soil water. Moreover, agriculture, primarily through N fertilizer and manure use, contributes nearly 70% of all anthropogenic nitrous oxide (N_2O) emissions[12]—a greenhouse gas almost 300 times more potent than carbon dioxide[13]. Precision agriculture, leveraging smart sensors, machine learning, artificial intelligence, and data-driven farm management, aims to optimize nutrient and water inputs, thereby improving productivity while minimizing environmental impacts[3,14,15]. Field-deployable sensing systems capable of continuously monitoring soil and plant nutrient status are therefore crucial for enabling timely, informed decisions in precision nutrient management.

Real-time monitoring of soil nutrients and crop biomolecules would enable early detection of drought and N stress by capturing dynamic changes in soil nutrient content as well as stress-associated phytohormones in plants. N and phytohormone signaling pathways are intricately connected, influencing plant growth and development through a complex network of interactions. Nitrate not only serves as a vital nutrient but also acts as a signaling molecule that triggers both local and systemic pathways, impacting gene expression, metabolism, physiology, and developmental processes[16]. These pathways are closely integrated with the biosynthesis, transport, and signaling of various plant defense hormones such as auxin, abscisic acid (ABA), ethylene (ET), salicylic acid (SA), Jasmonic acid (JA), and gibberellins[17–20]. Conversely, hormonal signaling can modulate nitrate-related regulatory networks, creating a feedback loop that fine-tunes plant's adaptation responses to environmental conditions. Recent studies have shown that the interplay between nitrate and numerous hormones coordinates critical aspects of plant growth, including root development, shoot branching, and stem cell dynamics. There is a strong connection between **auxin** and N in species like *Arabidopsis thaliana*, *Zea mays* (maize), and *Oryza sativa* (rice)[21–24]. Changes in N availability influence auxin transport and signaling, directly impacting root development. For instance, in rice, auxin accumulation (i.e., **Indole-3-acetic acid**, IAA) in roots is induced under partial nitrate nutrition compared to ammonium-only conditions[23]. Auxin signaling in response to nitrate, involving key genes like TAR2 and the auxin receptor AFB3, is crucial for both primary and lateral root growth[25]. The nitrate transceptor NRT1.1 also plays a significant role by regulating auxin transport. NRT1.1 negatively regulates auxin accumulation in lateral roots under low nitrate conditions, thereby preventing lateral root elongation and reducing the plant's capacity to forage effectively for nitrate and ammonium[21]. **Ethylene** (ET) is another hormone, which is regulated by the availability of N in the soil. Studies reveal that when *Arabidopsis* roots are exposed to high nitrate concentrations, ET production increases, downregulating the nitrate transporter NRT2.1 and upregulating the nitrate transceptor NRT1.1[26]. In another experiment suggesting a negative feedback loop, when seedlings were transferred from high (10 mM) to low (0.2 mM) nitrate conditions, there was a rapid burst of ET, which initially upregulated NRT2.1 gene expression, enhancing nitrate uptake and decreasing nitrate levels around the roots[27]. This reduction in the nitrate levels then triggered ET biosynthesis and signaling, ultimately causing the downregulation of NRT2.1. A potential link between nitrate and other phytohormones, such as **salicylic acid (SA)** and **methyl jasmonate (MeJA)**, a derivative of jasmonic acid, has been suggested in several studies. SA modulates nitrate uptake and assimilation,

as observed in *Citrullus lanatus L.* (watermelon), where SA increased nitrate uptake and assimilation by upregulating N reductase activity and influencing the expression of nitrate transporter genes[28]. JA, particularly its active form MeJA, often downregulates nitrate uptake under stress by prioritizing defense-related metabolism over nutrient acquisition. The **SA–JA crosstalk**[29] helps balance these processes through the *stress-initiated nitrate allocation to roots (SINAR)* mechanism, where JA and ET signaling upregulate NRT1.8 (nitrate transport into roots for detoxification) and downregulate NRT1.5 (nitrate export to shoots), while SA signaling modulates nitrate assimilation activity. Additionally, SINAR balances the trade-off between stress tolerance and plant growth, which depends on nitrate reductase activity[30]. These N-hormonal cross talks are summarized in **Fig. 1a** [29,31–42]. Thus, real-time monitoring of these hormones alongside plant and soil N would uncover the various regulatory mechanisms through which they interact under conditions of excess or deficiency in soil N levels.

Currently, established laboratory-based methods for measuring soil N and phytohormones include mass spectrometry, ultraviolet-visible spectrophotometry, ion chromatography, chemiluminescence, or metabolomics[43–47]. However, these techniques involve complex instrumentation and associated costs, along with labor-intensive procedures and lack real-time and spatiotemporal information. Metabolomics is a complex and tedious process that involves multiple steps, including sample extraction and preparation, analytical separation and measurement, data processing, metabolite identification, and biomarker discovery[48]. Colorimetric determination of ions requires extraction of ions from soil samples using a high-concentration (e.g., 2 M) KCl solution, limiting its practical operation in fields[49,50]. The ion-selective probes used for in-field monitoring lack the ability to multiplex (i.e., detect multiple ions and biomolecules with a single probe), lack wireless data transmission capabilities, and involve significant costs, particularly when several sensors need to be deployed in the field to achieve high-resolution spatiotemporal monitoring. Hence, wireless, multiplexed, and low-cost sensors are needed to collect high-frequency real-time information on plants and soil.

Recently, electrochemical sensors have gained popularity as low-cost alternatives for ion and hormone detection. The most effective method for measuring ion concentration remains the ion-selective membrane (ISM)-based approach, which uses solid contact electrodes with ion-to-electron transducing layers[51–57]. Strategies to enhance the electrode surface area include using laser-induced graphene electrodes that are modified with ion-specific ionophores[58]. Furthermore, various electrode modification schemes have been adopted to improve sensing performance. For example, additional coatings such as a polyhydroxyethylmethacrylate hydrogel layer[59] or polyvinyl butyral[60,61] are applied atop the AgCl reference electrode to maintain a stable reference potential. To improve the working electrode, materials such as multiwalled carbon nanotubes[62,63], macroporous carbon[64], polymer-carbon nanotube composites[65], or conjugated conducting polymers like polyaniline[66], poly(3,4-ethylenedioxythiophene) (PEDOT)[67], or poly(3-octylthiophene) (POT)[68] are added as solid-contact ion-to-electron transducing layers. PEDOT is particularly stable due to its ability to oxidize to $PEDOT^+$, which attracts lipophilic ions from the ion-selective layer[69]. Nonactin-based ionophores are commonly used in solid contact ion-selective electrodes (ISEs) for ammonium detection[70,71]. However, this method has drawbacks, such as interference from potassium ions[72], the fragile nature of the ISM, the high cost of nonactin ionophores, and biocompatibility concerns[73]. While numerous electrochemical sensors for selective phytohormone detection are documented in the literature[74–77], only a few are designed as

crop-wearable devices for *in situ* hormone monitoring. Our research group has developed crop-wearable and *in situ* sensors featuring flexible tattoo-like or 3D-printed needle-like structures with their working electrodes modified by non-enzymatic composites, such as copper-based metal-organic framework for SA detection[78–82], gold nanoparticle decorated graphene hydrogel nanocomposite for IAA detection[79,81], and copper complex (I) coating for ET detection[82,83]. However, an integrated platform that simultaneously monitors both soil and crop conditions to synchronize soil nutrient supply to crop demand is still lacking.

In this work, we introduce a multiplexed sensor suite capable of simultaneously measuring soil N levels as well as crop N and phytohormone levels. The plant and soil sensor suite is composed of three custom-designed modules (**Fig. 1b**) that collectively enable real-time monitoring of key physiological and soil parameters. Stem Module-1 incorporates microneedles arranged on two sides of a rectangular structure, enabling detection of SA, IAA, MeJA, and pH, along with a central chamber for ET accumulation and sensing. Stem Module-2 adds potentiometric sensors for nitrate (NO_3^-) and ammonium (NH_4^+) detection within the plant stem, using microneedles configured as reference and working electrodes. Collectively, we have named the stem modules as **Stem-FIT**, serving as a "fitness tracker" for the plant stem. Complementing these, the Soil Module (or **Soil-FIT**, serving as a "fitness tracker" for the soil) integrates potentiometric sensors for pH, NO_3^-, and NH_4^+ at multiple depths (1, 5, and 10 cm), providing a spatial profile of soil nutrient status. Soil pH, a key factor in N availability, affects microbial activity and nutrient accessibility, with an optimal range of 5.5-7.5 being ideal for regulating these processes[84,85]. Therefore, real-time, simultaneous measurement of soil N content, plant N uptake, and pH adjustments would help synchronize N supply with crop demand. Collectively, these modules constitute the multiplexed plant–soil sensor suite, which was thoroughly characterized for sensitivity, repeatability, drift, and selectivity. The sensor suite was further validated in live bell pepper plants exposed to water and N stress, enabling real-time monitoring of plant hormones, plant N, and soil N levels. All recorded hormone and N measurements were adjusted for pH to ensure accuracy. Unlike conventional methods that are discrete, invasive, and lack temporal resolution, this integrated sensor platform successfully captured the dynamic changes in these parameters continuously and in real time. In addition, coupling the sensor data with a long short-term memory (LSTM) model enabled accurate short-term forecasting of N and hormone fluctuations under both irrigated and water-stressed conditions. The LSTM framework not only tracked real-time variability with high fidelity but also anticipated future shifts in N and hormone levels, providing predictive insight into plant stress responses. Such predictive capability is critical for early stress detection, allowing proactive management decisions that optimize N application, improve crop resilience, and minimize environmental impacts.

In summary, the key contributions of this work include the following:

- A sensor suite that enables in-situ and real-time measurements of four stress-associated plant phytohormones SA, IAA, MeJA, ET, and two crucial nutrients (nitrate and ammonium) in both plant and soil.
- Hormone and nutrient measurements corrected at different pH levels.
- Measurement of nitrate and ammonium ions at three depths in the soil.
- Integration of sensor data with an LSTM model to forecast nutrient and hormone fluctuations, enabling early detection of plant stress and supporting predictive precision agriculture.

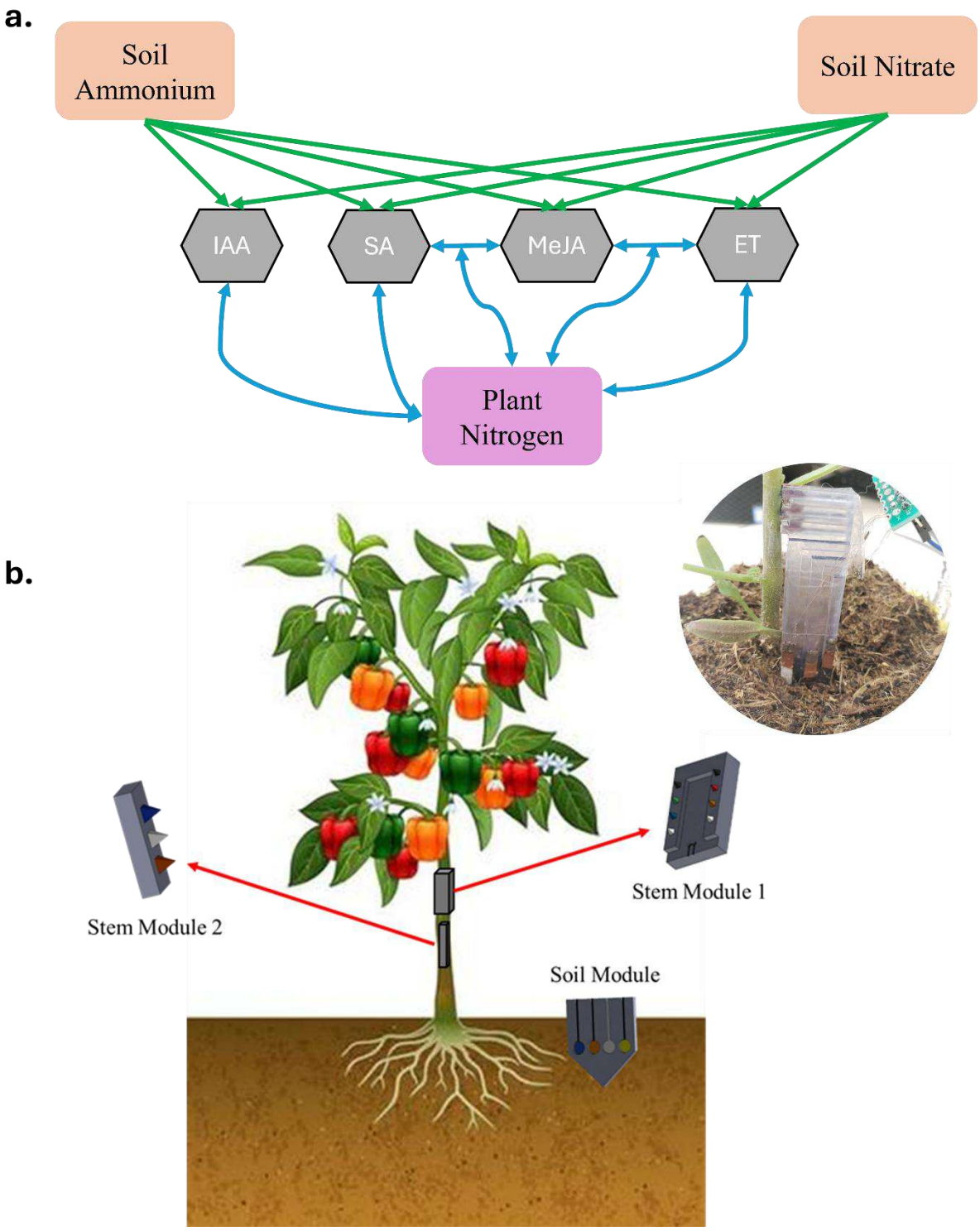

Fig. 1: (a) Crosstalk between the plant phytohormones SA, MeJA, IAA, and ET and sap and soil N (i.e., nitrate and ammonium), illustrating the regulatory interactions within the N–hormone signaling network. (b) Conceptual deployment of the developed sensor modules, showing sensors positioned both in the root zone for soil measurements and on the stem for sap monitoring. The inset in the upper-right corner of (b) displays the actual integrated stem and soil sensor suite attached to a plant.

2. Materials and Methods

2.1 Sensor Fabrication

The sensor suite was fabricated via 3D printing with biocompatible materials and functionalized with optimized coatings to ensure precise and selective measurements. The fabrication and chemical functionalization processes are explained in **Supplementary Note 1** and illustrated in **Fig. S1**.

2.2 Data Acquisition for Sensor Characterization and Testing Experiments

Electrochemical techniques were utilized to characterize SA, IAA, and MeJA sensors. These are three electrode-based amperometric sensors (**Supplementary Note 2**). Differential pulse voltammetry (DPV) was applied in all cases. The EmStat4S potentiostat from BaSi Inc. was used for running these DPV analyses.

DPV Settings:

- SA: The DPV was conducted from -1.0 V to 1.6 V with a step voltage of 0.01 V and a scan rate of 10 mV/s. The amplitude and time interval of the input pulse were 0.3 V and 0.1 s, respectively. The concentration range for SA calibration was 0.1 μM to 1000 μM.
- IAA: DPV was conducted from 0 V to 1.6 V with the same step voltage, scan rate, amplitude, and time interval. The calibration range for IAA was 0.1 μM to 200 μM.
- MeJA: DPV was conducted from 0.8 V to 1.5 V with identical step voltage, scan rate, amplitude, and time interval. The calibration range for MeJA was 0.5 μM to 200 μM.

In contrast, ET and pH sensors are two electrode-based resistive sensors, with the resistance variation across the electrodes converted into a voltage signal through a voltage divider (**Supplementary Note 2**). The data acquisition and processing procedures are described in our previous work[82,83]. The nitrate and ammonium sensors operate as two-electrode potentiometric systems, with detailed information on their data logging provided in our earlier publications[86].

For calibration of the stem modules, plant sap was spiked with varying concentrations of the target analyte. Sap was obtained by cutting and squeezing the plant stems, followed by purification through centrifugation (Eppendorf Model 5804R, Hamburg, Germany). The sap pH was maintained at 7.1 for all experiments. For calibration of the soil module, nitrate- and ammonium-enriched soil samples were prepared by adding stock salt solutions ($NaNO_3$ for nitrate and $(NH_4)_2SO_4$ for ammonium) to soil–water mixtures. The soil was first sun-dried for 5 hours, after which 50 g of dried soil was combined with 25 mL of water in individual containers. Small volumes of the stock solutions were then incrementally added to achieve the desired nitrate and ammonium concentrations, which were validated using a commercial multi-ion system (NT Sensors, Vila-seca, Spain). For ET sensor calibration, a custom gas-sensing system was developed, consisting of mass flow controllers, calibration gas cylinders, and a sensing chamber housing the sensor[83,87,88]. Various ET concentrations were introduced into the chamber by adjusting the ET gas

flow rate while maintaining a constant flow of the dilution gas (N_2). The flow controllers regulated the gas flow, and mass flow meters monitored it in real time. ET concentrations were determined based on the measured flow rates and the chamber volume. For calibration of the pH sensor, a range of pH solutions was prepared using a commercial pH meter (Mettler Toledo, Columbus, OH).

2.3 Real-time Measurements in Live Plants

The sensors were tested in live bell pepper plants. The needle-structured Stem Module-1 and Stem Module-2 (**Fig. 1**) were installed into the stem of the plants. Simultaneously, the Soil Module (**Fig. 1**) was inserted in the soil to measure nitrate and ammonium levels at 1, 5, and 10 cm of depths. The sensors recorded measurements every 3 hours, resulting in 8 measurements per day. We used 4 treatment groups, each with 10 plant replications, totaling 40 pots of plants. The treatments are listed in **Table I**. Two water treatments were applied: fully irrigated (100%) and deficit irrigated (50%). Within each water treatment group, two N levels were used: medium and high. For the medium N treatment, about 125 ml of $NaNO_3$ solution was added to the pots on Day 1, Day 11, Day 13, and Day 15. For the high N treatment, around 500 ml of $NaNO_3$ solution was added on Day 1, followed by 125 ml on Day 11, Day 13, and Day 15.

Table I: List of treatment groups used in this study

Water application	**N application**	
No water stress or control (fully irrigated-100%)	Medium N (125 ml of $NaNO_3$)	High N (500 ml of $NaNO_3$ followed by 125 ml)
Water stress (deficit irrigation-50%)	Medium N (125 ml of $NaNO_3$)	High N (500 ml of $NaNO_3$ followed by 125 ml)

2.4 Machine Learning-based Prediction

We selected an LSTM-based framework for prediction because LSTM networks are particularly effective for sequential and time-series data, as they can capture long-range temporal dependencies and nonlinear interactions better than traditional machine learning models such as linear regression, decision trees, or support vector machines. Unlike standard recurrent neural networks (RNNs), LSTMs include gated mechanisms (input, forget, and output gates) that mitigate vanishing and exploding gradient problems, making them well suited for modeling complex plant physiological signals that evolve over days under varying environmental conditions.

All LSTM-based prediction modeling was implemented in Python 3.12 using Jupyter Notebook (JupyterLab interface). Data preprocessing, scaling, and evaluation employed scikit-learn v1.5, while deep learning models were constructed and trained using TensorFlow v2.16 and Keras v3.0. First, the data worksheet was loaded, and the Day column was selected as the x-axis along with a

target variable (e.g., nitrate, ammonium, IAA, SA, MeJA, or ET). The target series was scaled to the range [0,1] using MinMaxScaler to ensure stable training across different magnitudes. From this normalized series, supervised sequences were generated by applying a sliding window of 10 past points (seq_length=10), where each input sample consisted of a 10-step history and the corresponding label was defined as the value of the target variable at the next time step. With approximately 20 days of data, this approach resulted in an 18-day training set and a 2-day testing set (90/10 split after sequence generation). The LSTM model employed a compact architecture of two stacked LSTM layers (50 units each) with a dropout rate of 0.2 to reduce overfitting, followed by a dense layer with 25 units and ReLU activation, and a single linear output neuron. The network was compiled using the Adam optimizer (learning rate = 0.001) and trained using mean squared error (MSE) loss for 50 epochs with a batch size of 16. After training, predictions were generated for the testing sequences and inverse-transformed back to the original units (ppm or μM). Finally, the predicted values and actual measurements were aligned with their respective dates and visualized in a plot containing three curves: training data, testing data, and model predictions.

3. Results and Discussion

The surface morphology and chemical composition of the coatings were examined using scanning electron microscopy (SEM), Fourier Transform Infrared (FTIR) spectroscopy, ultraviolet-visible (UV-Vis) spectroscopy, and Nuclear magnetic resonance (NMR) spectroscopy. The details are outlined in **Supplementary Note 3** and illustrated in **Fig. S2**.

3.1 Sensor Calibration

The DPV plot for SA calibration shows two major peaks (**Fig. 2a**). The first peak, at -0.2 V, corresponds to the reduction of CuMOF, while the second peak, near 0.85 V, is due to the oxidation of SA. The Cu^{2+} ion reduction facilitates the oxidation of SA. Notably, as the CuMOF peak decreases, the SA peak increases. The separation between the two peaks is approximately 1.05 V, and the ratio of these peak currents serves as the response signal. The peak current for the IAA sensor appears at 0.85 V and increases with higher IAA concentrations (**Fig. 2b**). Likewise, the peak current for the MeJA sensor is observed at 1.23 V and increases with higher MeJA concentrations (**Fig. 2c**).

Calibration curves for SA, IAA, and MeJA (**Fig. 2d-f**) were fitted with power series, while the calibration curve for nitrate (i.e., potential versus nitrate concentration in the log scale) was fitted with a polynomial fit (**Fig. 2h, k**). On the other hand, calibration curves for ethylene, ammonium, and pH sensors were fitted with linear lines (**Fig. 2g, i, j, l**). Nitrate and ammonium concentrations were measured in both plant sap and soil. Hence, these sensors had two calibration plots, one in soil and another in plant sap.

3.2 Sensitivity and LOD Analysis

To determine the sensitivity of SA, IAA, and MeJA sensors with calibration curves fitted using power series ($y = ax^b + c$), the derivative (abx^{b-1}) of the fitted curve equation is calculated. For the nitrate sensor, which is fitted with a second-order polynomial ($y = ax^2 + bx + c$), the derivative (2ax + b) is used to measure sensitivity. Sensitivity is assessed at both the upper and lower concentration limits for SA, IAA, MeJA, and nitrate ion sensors using the method described in previous research[82,89].

For sensors with linear calibration curves ($y = mx + c$) such as those for ammonium, ethylene, and pH, sensitivity is determined using the slope (m) of the linear fit. The limit of detection (LOD) for SA, IAA, MeJA, ethylene, pH, nitrate, and ammonium sensors is calculated using the formula:

$$LOD = \frac{3*std.dev}{Sensitivity} \quad (1)$$

The sensitivity and LOD values for nonlinear sensors are provided in **Table II**, while the sensitivity and LOD for linear sensors are listed in **Table III**.

Table II: Performance metrics of non-linear sensors.

Sensor	Equation	Low Concentration Sensitivity	High Concentration Sensitivity	LOD
Salicylic acid, SA	$I_{SA}/I_{CuMOF} = 0.0144(SA)^{0.38} + 0.8431$	0.0228 μM^{-1} (at 0.1 µM)	7.5 x 10^{-5} μM^{-1} (at 1000 µM)	1.315 µM
Indole-3-acetic acid, IAA	$I = 1.03(IAA)^{0.75} + 44.23$	1.373 µA μM^{-1} (at 0.1 µM)	0.205 µA μM^{-1} (at 200 µM)	0.218 µM
Methyl jasmonate, MeJA	$I = 23.39(MeJA)^{0.006}$	0.279 µA μM^{-1} (at 0.5 µM)	7.24 x 10^{-4} µA μM^{-1} (at 200 µM)	1.07 µM
Nitrate, NO_3^-	$E=-35.96(\text{Log}NO_3)^2 + 27.255LogNO_3 - 107.18$	-8.705 mV/ Log(ppm) (at 0.5 Log(ppm) or 3.16 ppm)	-224.46 mV/ Log(ppm) (at 3.5 Log(ppm)	1.08 ppm

			or 3162.27 ppm)	

Table III: Performance metrics of linear sensors.

Sensor	Equation	Sensitivity	LOD
Ethylene, ET	R =1.034 ET + 1.30571	1.034 kΩ/ppm	0.29 ppm
Ammonium, NH_4^+	E=39.157$LogNH_4$+564.41	39.157 mV/ Log(ppm)	1.017 ppm
pH	R =28. 682pH + 4.3739	28. 682 kΩ/pH	0.01 pH

The sensors were also extensively characterized for repeatability, drift, selectivity, and dynamic response, which are described in **Supplementary Notes 4, 5** and presented in **Figs. S3-S7**.

3.3 pH Correction

All sensors, with the exception of the pH and ET sensors (the latter does not directly contact plant sap and is therefore unaffected by pH), are adjusted to compensate for pH variations. This correction is necessary because the pH of plant sap and soil can change over time, affecting sensor responses. For instance, **Fig. 3** shows the variations in the calibration plots for the SA, IAA, MeJA, nitrate, and ammonium sensors with different pH levels. The SA, MeJA, and ammonium sensors demonstrate a coefficient of variation of about 2% due to pH changes. Hence, pH correction was done based on methods outlined in our previous work[82]. The correction factor includes slope, exponent, and intercept, which are calculated with respect to a standard pH value using the following equations:

$$f_{intercept} = \frac{intercept(pH)}{intercept(\text{pH 7.1})} \quad (2)$$

$$f_{slope} = \frac{slope(pH)}{slope(\text{pH 7.1})} \quad (3)$$

$$f_{exponent} = \frac{\boldsymbol{exponent(pH)}}{\boldsymbol{exponent(\text{pH 7.1})}} \quad (4)$$

The corrected intercept, slope and exponent for each sensor are calculated based on the following equations:

$$intercept(corr.) = f_{intercept} * intercept(init.) \quad (5)$$

$$slope(corr.) = f_{slope} * slope(init.) \quad (6)$$

$$exponent(corr.) = f_{exponent} * exponent(init.) \quad (7)$$

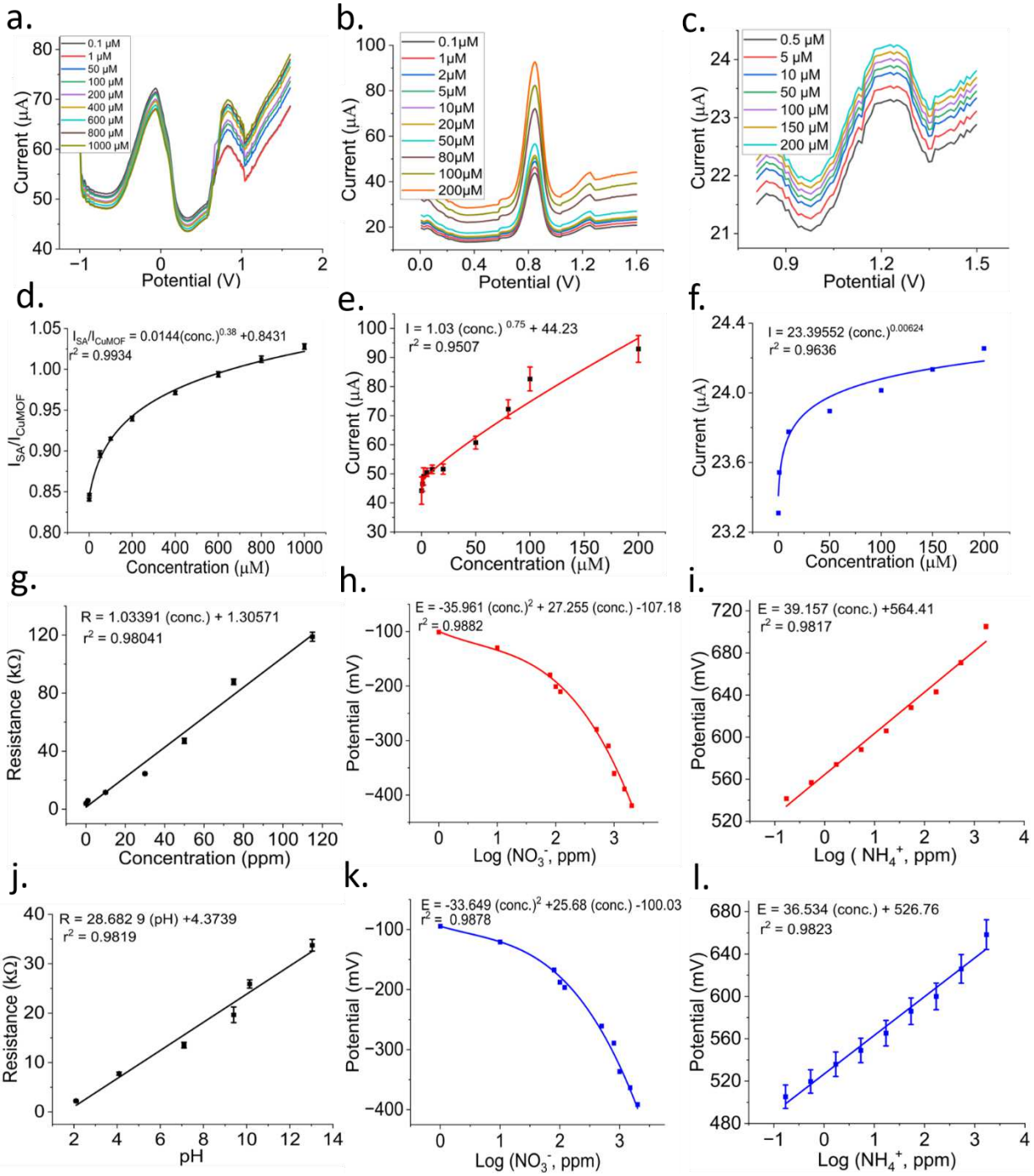

Fig. 2: Differential Pulse Voltammetry of (a) SA, (b) IAA, and (c) MeJA sensors. Calibration curves of (d) SA, (e) IAA, and (f) MeJA sensors. Calibration curves of (g) ethylene sensor, (h) nitrate sensor in plant sap, and (i) ammonium sensor in plant sap. Calibration curves of (j) pH sensor, (k) nitrate sensor in soil, and (l) ammonium sensor in soil.

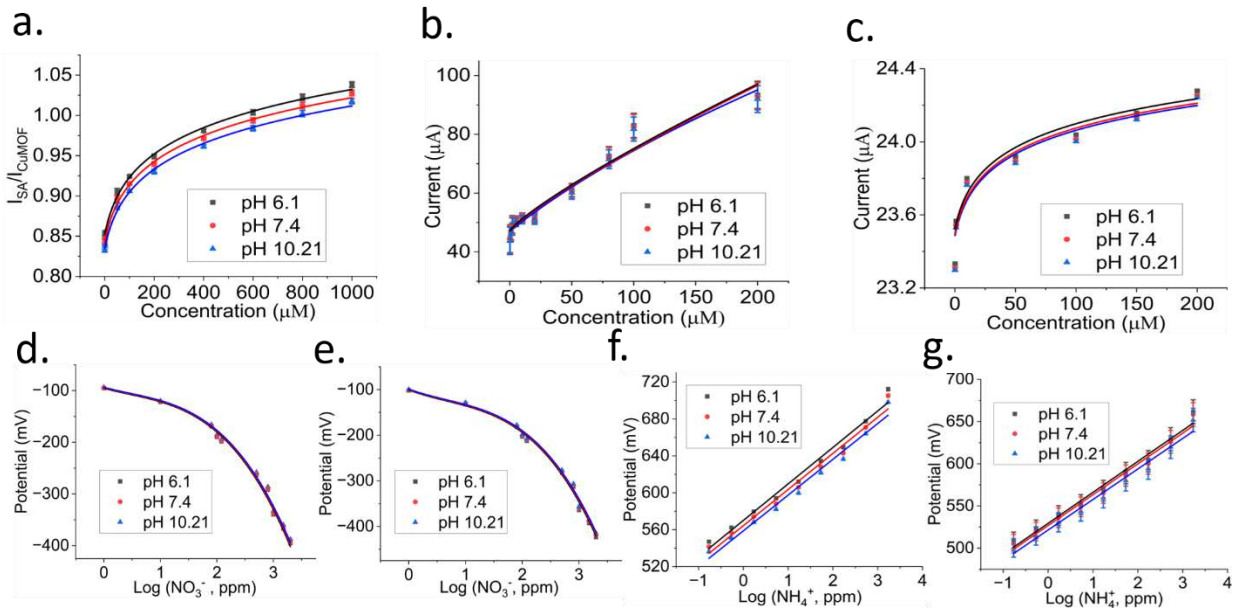

Fig. 3: Calibration curves of (a) SA sensor, (b) IAA sensor, (c) MeJA sensor, (d) nitrate sensor in sap, (e) nitrate sensor in soil, (f) ammonium sensor in sap, and (g) ammonium sensor in soil with varying pH levels.

3.4 Real-time Plant and Soil Measurements

The sensors were tested in live bell pepper plants. For the medium N treatment, soil nitrate and ammonium levels, measured using both our sensors and a commercial NPK probe (Honio, China), are shown in **Fig. 4**. Following the application of $NaNO_3$ (as detailed in the Methods section), soil nitrate and ammonium levels exhibited sharp increases followed by gradual declines, appearing as distinct stepwise rises on Day 1, Day 11, Day 13, and Day 15. **Fig. 5** shows the NO_3^--N, NH_4^+-N, and hormone levels in the plant sap measured with the needle sensors. The NO_3^--N levels were lower in water-stressed plants than in controls due to reduced soil water content and hence decreased NO_3^- uptake by the stressed plants. These findings provide crucial insights into plant NO_3^- variability based on soil water availability. After Day 12, NO_3^--N levels in the plants subsided and finally plateaued despite additional fertigation on Days 13 and 15, supporting literature that plants only absorb 30-50% of the applied fertilizer[90]. The NH_4^+-N levels in both soil and plants followed the same trend as NO_3^--N. In contrast, the hormone levels increased in water-stressed plants and declined in irrigated plants (control). This hormonal trend aligns with findings in the literature. Studies show that endogenous JA levels rise during water deficit and act together with abscisic acid (ABA) to prime drought acclimation[91,92]. Various reports have demonstrated accumulation of endogenous SA (and JA) under abiotic stresses, including drought, across species/tissues[93,94]. In contrast, auxin (IAA) responses to drought are species- and tissue-specific and sometimes inconsistent across studies. Some reports show decreases in whole-plant free auxin under prolonged drought while others (especially in root apices) document short-term local increases[95]. These complex hormonal shifts help the plant manage water scarcity, balancing growth and survival during prolonged periods of drought or

water stress. Our sensor suite has the capability to directly measure their levels in the plant in real-time.

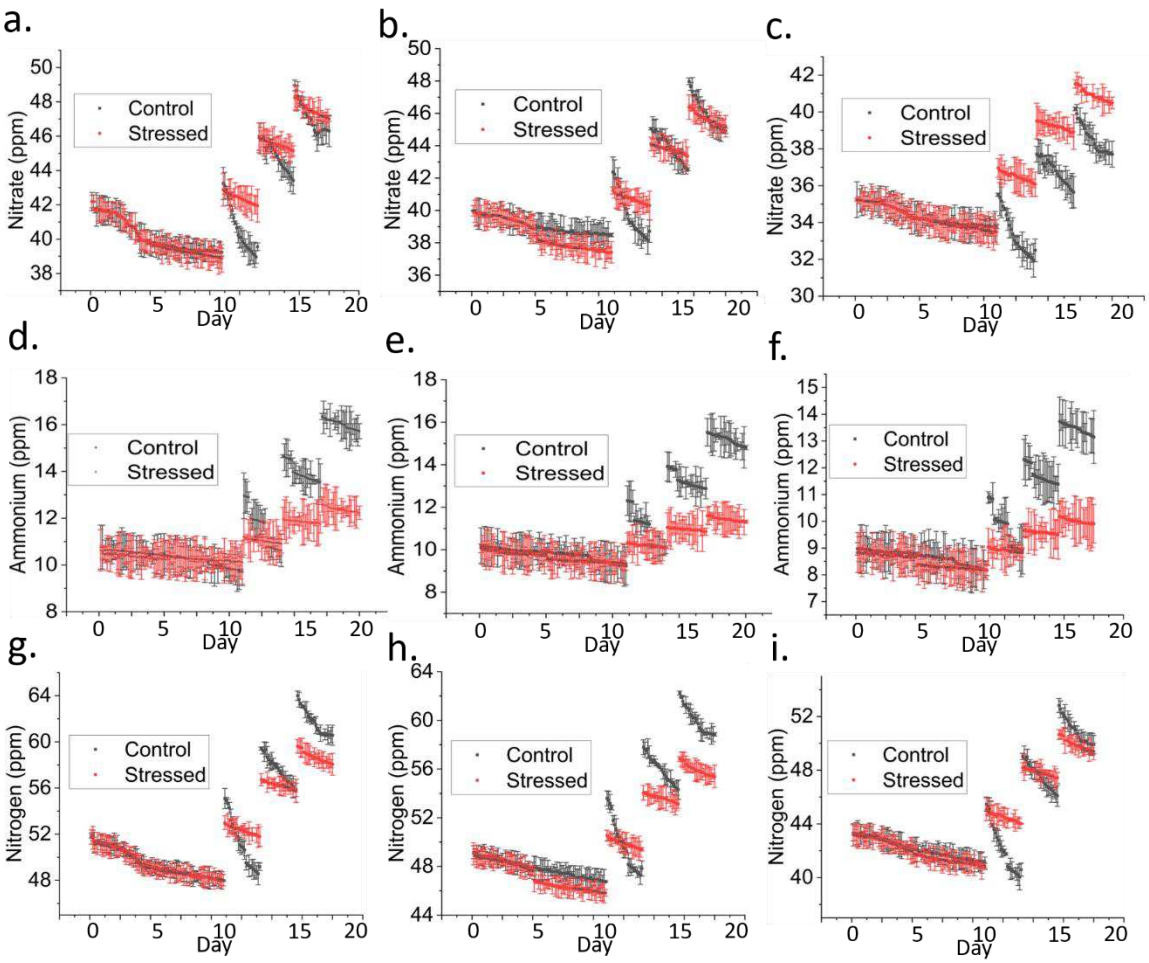

Fig. 4: Nitrate-N levels measured at different soil depths with our sensor: (a) 1 cm, (b) 5 cm, and (c) 10 cm. Ammonium-N levels measured at different soil depths with our sensor: (d) 1 cm, (e) 5 cm, and (f) 10 cm. Total N measurements at various depths using a commercial NPK probe: (g) 1 cm, (h) 5 cm, and (i) 10 cm. In all these cases, the soil was treated with a medium level of N.

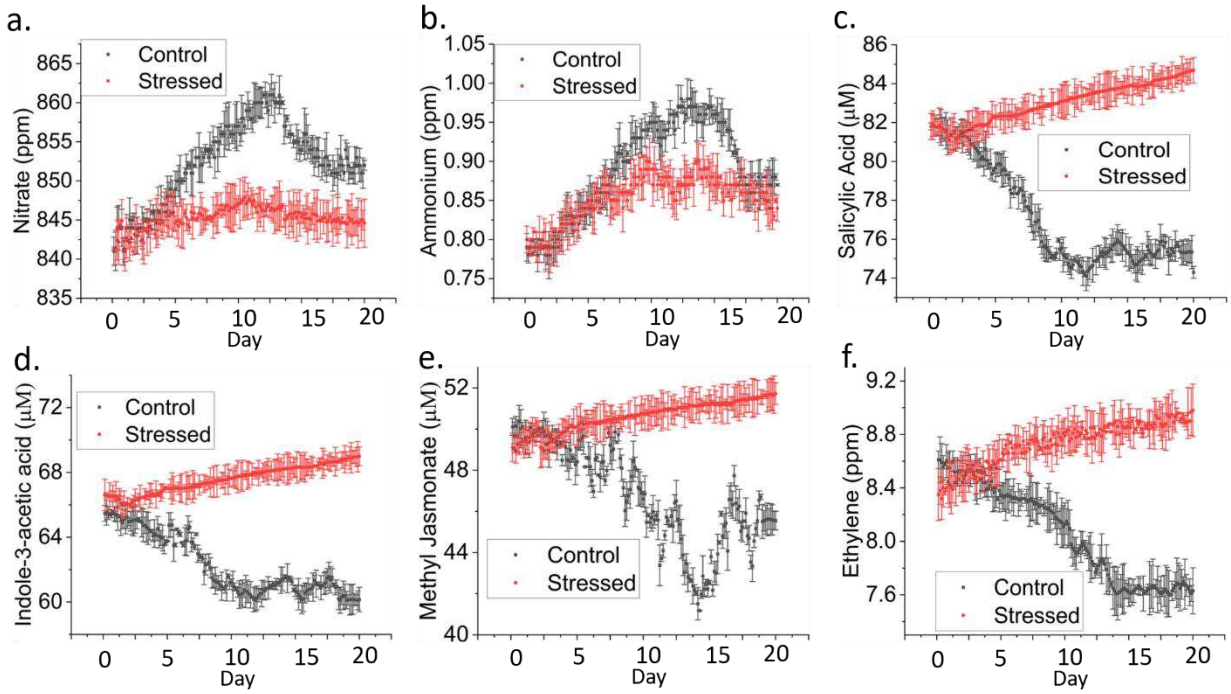

Fig. 5: Twenty days of continuous monitoring of (a) nitrate-N, (b) ammonium-N, (c) SA, (d) IAA, (e) MeJA, and (f) ethylene levels in both control (fully irrigated) and water stressed (deficit irrigated) plants, when the soil was treated with medium levels of N.

For the high N treatment, the trends in the NO_3^--N, NH_4^+-N, and hormone levels were not as nuanced as those observed in the medium N treated plants. The results are depicted in **Fig. 6** and **7**. This reduced sensitivity is likely due to N toxicity[96], which occurs when N levels greatly exceed the plant's capacity to absorb it. Excessive N can lead to leaf burns, where leaves appear scorched, and chlorosis, characterized by yellowing. This happens because high N disrupts photosynthesis and promotes excessive foliage growth, increasing the plant's water needs and making it more susceptible to drought and other environmental stresses. The observed chlorosis and heightened sensitivity to environmental stress in the high N-treated plants in this work resulted in less distinct molecular differences between control and water-stressed plants.

The aforementioned results indicate that our crop-wearable sensor suite plays a pivotal role in revealing not only the release kinetics of phytohormones and their crosstalk with nitrate uptake in plants in real time, but also for detecting the onset of N toxicity. This would enable timely intervention to mitigate or even revert the adverse effects of N toxicity in plants.

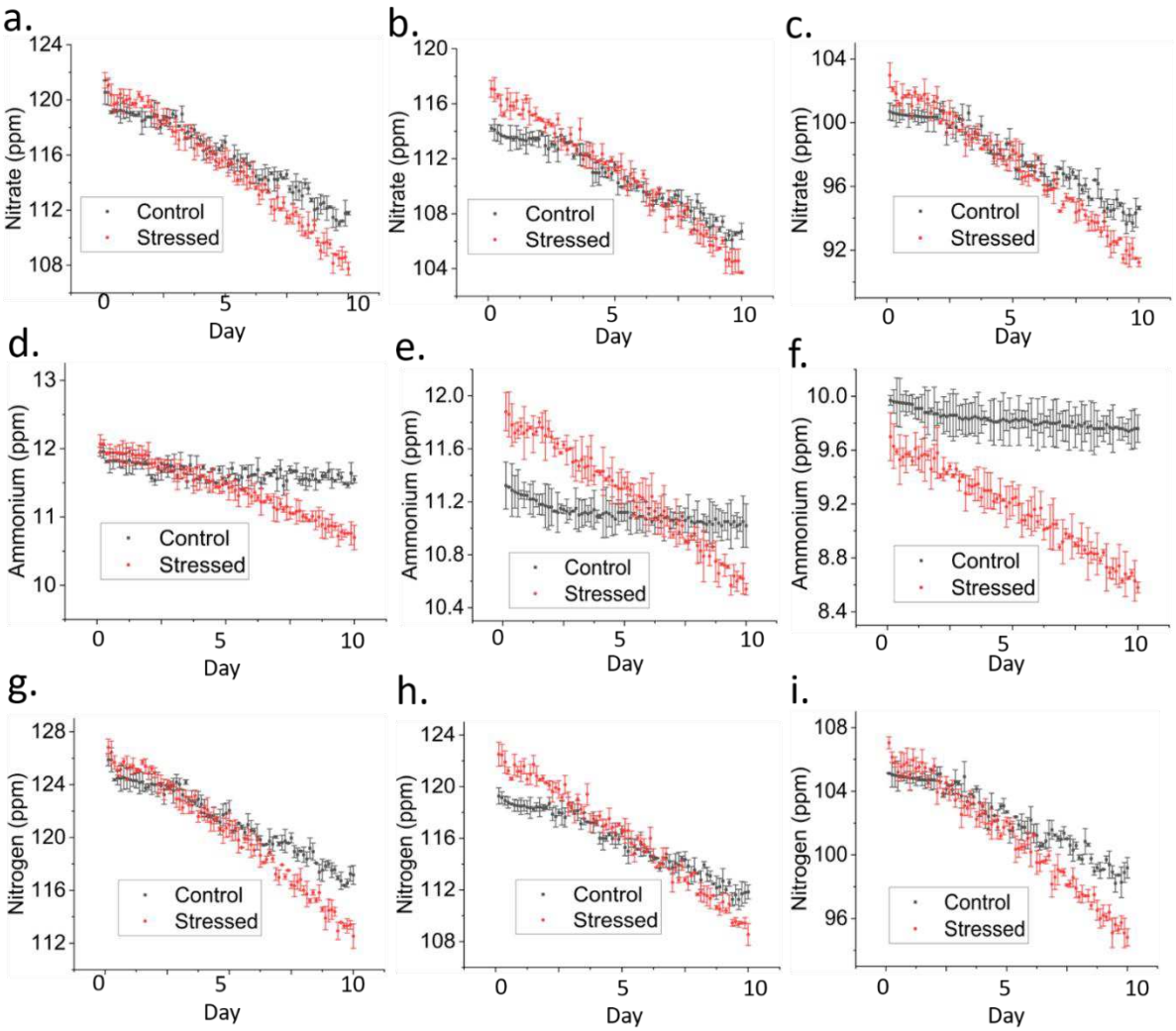

Fig. 6: Nitrate-N levels measured at different soil depths with our sensor: (a) 1 cm, (b) 5 cm, and (c) 10 cm. Ammonium-N levels measured at different soil depths with our sensor: (d) 1 cm, (e) 5 cm, and (f) 10 cm. Total N measurements at various depths using a commercial NPK probe: (g) 1 cm, (h) 5 cm, and (i) 10 cm. In all these cases, the soil was treated with a high level of N.

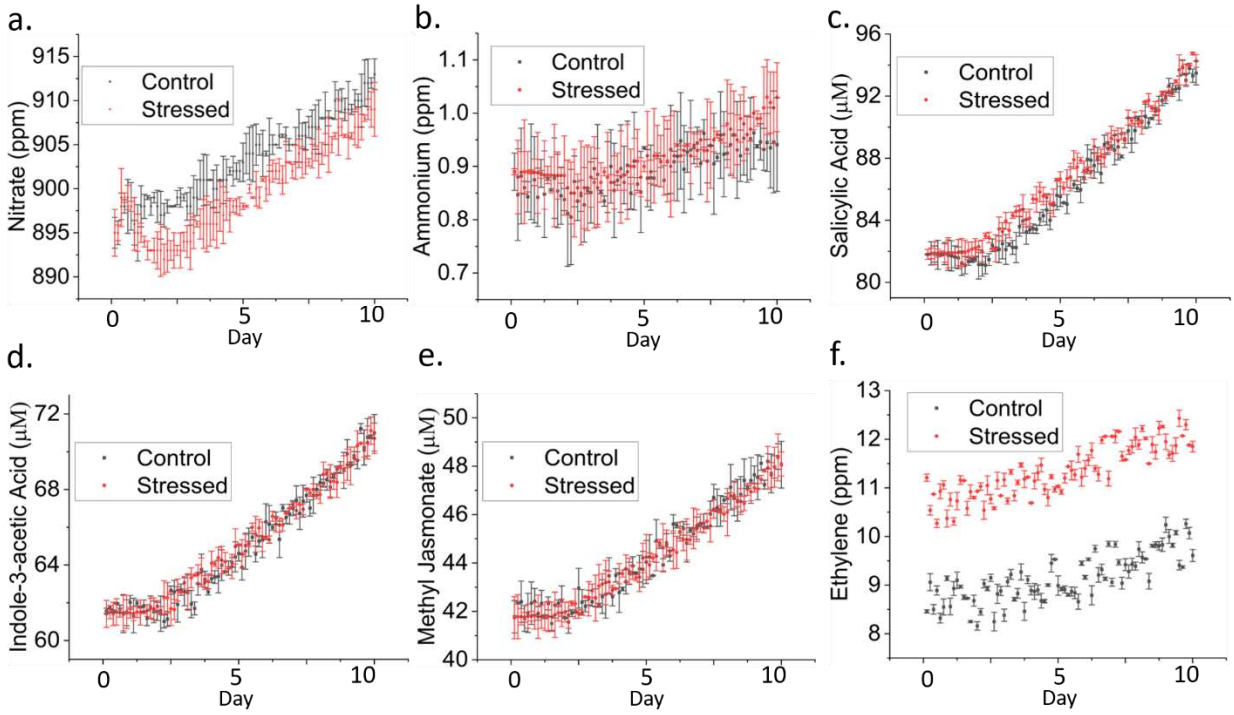

Fig. 7: Ten days of continuous monitoring of (a) nitrate-N, (b) ammonium-N, (c) SA, (d) IAA, (e) MeJA, and (f) ethylene levels in both control (fully irrigated) and water stressed (deficit irrigated) plants, when the soil was treated with a high level of N.

3.5 Sensor Validation Against Standard

The total N available in the soil was measured using a commercial NPK probe (see **Fig. 4g-i**). The results showed that the total N closely corresponded to the combined levels of NO_3^--N (**Fig. 4a-c**), NH_4^+-N (**Fig. 4d-f**) in the soil, as measured with our sensors. Additionally, as shown in **Supplementary Fig. S8**, the time-series measurements of hormone and nutrient levels obtained from our stem modules were validated using a high-performance liquid chromatography (HPLC) system from Shimadzu, Kyoto, Japan. The HPLC setup included a Shimadzu LC-10ATvp liquid chromatographic pump, a ZIC-HILIC SeQUANT PEEK-lined stainless-steel column (250 mm × 4.6 mm, 5 µm, 200 A^0), a Shimadzu SPD-10Aº detector set at 201 nm, and a 7125 injector equipped with a 50 µL sample loop. Small sap samples were collected daily and analyzed using HPLC to determine the analyte concentrations. Our sensors accurately estimated SA, IAA, MeJA, nitrate, and ammonium levels in both control and water-stressed plants, with a high Pearson correlation coefficient greater than 0.98, demonstrating excellent reliability. We adopted an indirect approach to validate the accuracy of our ethylene sensor, as outlined in a previous work[82]. Our ethylene sensor also demonstrated highly accurate results with a Pearson correlation coefficient of 0.99. The high Pearson correlation coefficients may be due to the relatively small sample size (around 10). Future studies will aim to validate the findings using a larger dataset with more than 100 samples. Unlike traditional mass spectroscopy and chromatography, which requires costly equipment, complex sampling, and skilled technicians, our crop-wearable sensor

suite enables real-time, in situ monitoring and early stress detection in live plants. Furthermore, the miniaturized needle structure of our sensors allows them to easily conform to delicate plant stems, unlike rigid commercial integrated circuits.

3.6 LSTM-based Plant Stress Prediction

The LSTM prediction framework demonstrated strong performance in capturing both temporal dynamics and treatment-specific variations of nitrate, ammonium, and phytohormone concentrations under medium N application. For the control (fully irrigated) plants (**Fig. 8a–f**), the model accurately followed the overall rise and decline patterns across the 20-day monitoring period. During the testing phase (last 2 days), the root mean square error (RMSE) for nitrate, ammonium, and ET predictions was below 0.5 ppm, while for SA, IAA, and MeJA, it remained under 0.4 μM. The nitrate and ammonium concentrations (**Fig. 8a–b**) were predicted with high fidelity, reflecting the model's ability to learn nutrient uptake patterns under consistent irrigation. Similarly, for SA, IAA, MeJA, and ET (**Fig. 8c–f**), the LSTM preserved the inherent fluctuations, indicating that the sensor readings were not only reproducible but also that the neural network could generalize physiological responses of the plants to soil conditions. The close alignment of red (actual) and green (predicted) traces highlights the robustness of the sensor–model integration in forecasting short-term nutrient and hormone dynamics.

In contrast, the stressed (deficit-irrigated) plants (**Fig. 8g–l**) revealed more pronounced fluctuations and distinct trajectories compared to control conditions, which were also effectively captured by the LSTM model. Nitrate and ammonium concentrations (**Fig. 8g–h**) showed slower upward trends, consistent with restricted nutrient mobility under water deficit, and the model closely tracked these altered patterns. Stress-related hormonal responses, including elevated SA and MeJA and shifts in IAA and ET levels (**Fig. 8i–l**), were reflected in both the observed data and the predictions, underscoring the physiological differences between treatments. Importantly, the model maintained prediction accuracy despite the increased variability in stress conditions, as evidenced by the tight overlap of predicted and actual curves during the testing window. Together, these results demonstrate that the combination of in-situ microneedle sensor data with LSTM modeling can accurately discriminate treatment effects while providing reliable short-term forecasts of both nutrient and hormonal dynamics.

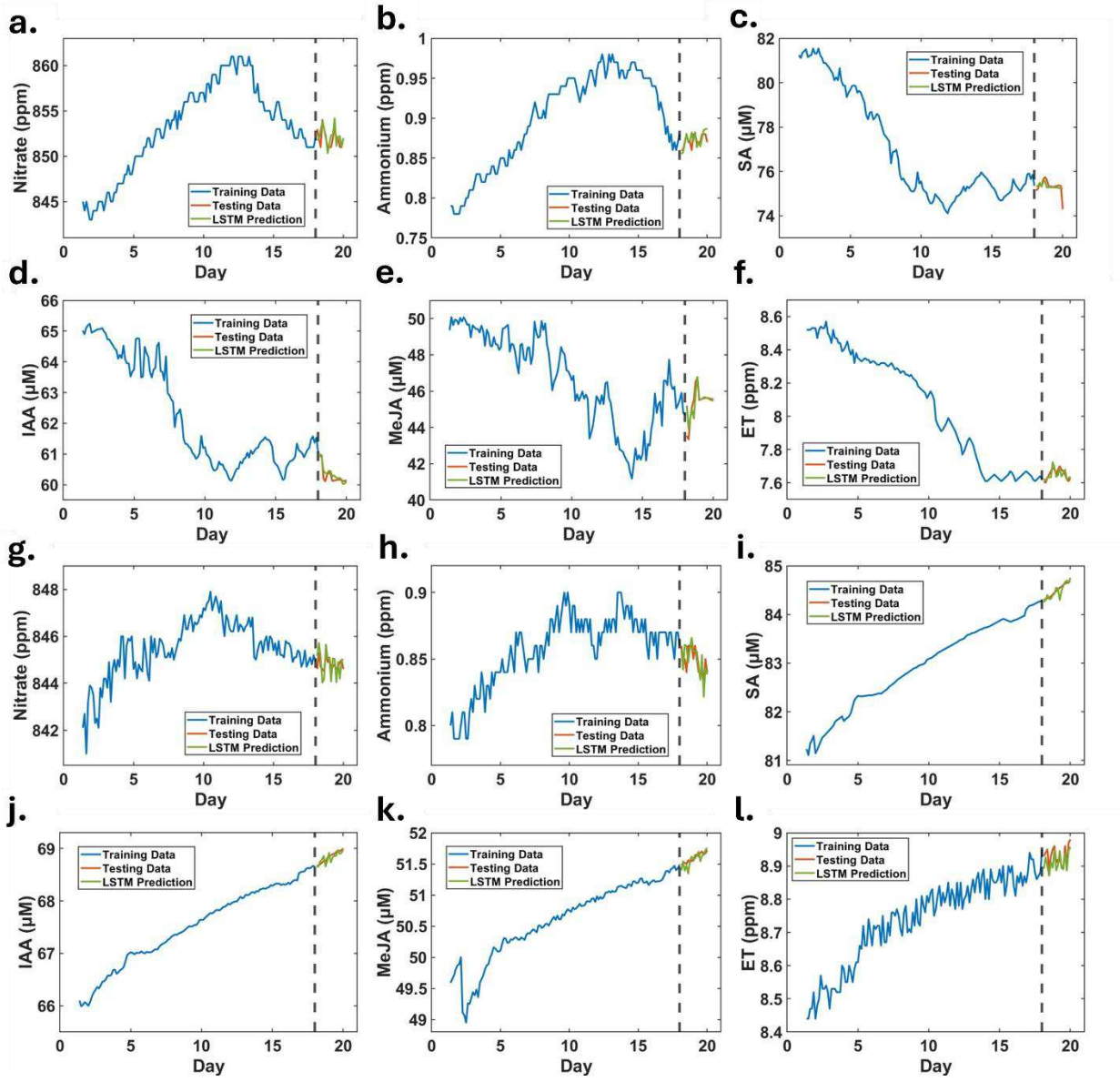

Fig. 8: LSTM prediction of (a) nitrate (control), (b) ammonium (control), (c) SA (control), (d) IAA (control), (e) MeJA (control), and (f) ethylene (control), using 18 days of training data and 2 days of prediction in fully irrigated (control) plants treated with medium levels of N. LSTM prediction of (g) nitrate (stress), (h) ammonium (stress), (i) SA (stress), (j) IAA (stress), (k) MeJA (stress), and (l) ethylene (stress), using 18 days of training data and 2 days of prediction in deficit irrigated (stress) plants treated with medium levels of N.

Table IV: Performance metrics of the LSTM-based prediction model for control and stress treatments under medium level of applied nitrate

	Ammonium Control	**Nitrate Control**	**Ethylene Control**	**IAA Control**	**MeJA Control**	**SA Control**
R^2	0.81	0.79	0.69	0.83	0.79	0.8
RMSE	0.004 ppm	0.41 ppm	0.02 ppm	0.12 µM	0.35 µM	0.09 µM
	Ammonium Stress	**Nitrate Stress**	**Ethylene Stress**	**IAA Stress**	**MeJA Stress**	**SA Stress**
R^2	0.79	0.78	0.81	0.85	0.75	0.86
RMSE	0.006 ppm	0.36 ppm	0.02 ppm	0.06 µM	0.08 µM	0.07 µM

Table IV summarizes the prediction performance of the LSTM model for ammonium, nitrate, ethylene, IAA, MeJA, and SA concentrations under both control (fully irrigated) and stress (deficit irrigated) conditions under medium level of applied nitrate. The coefficient of determination (R^2) values indicate strong model fit across all analytes, ranging from 0.69 to 0.86, with higher values observed for IAA and SA predictions in both treatments. Root mean square error (RMSE) values remained low, confirming high prediction accuracy, with ethylene exhibiting the lowest error (0.02) under both conditions. Notably, nitrate predictions showed slightly higher RMSE (0.41 in control and 0.36 in stress), reflecting the greater variability in nitrate dynamics compared to other analytes. Overall, the metrics demonstrate that the LSTM framework reliably captured both nutrient and hormone fluctuations, with comparable performance under irrigated and water-stressed conditions.

4. Conclusion

This study presented a multiplexed plant–soil sensor suite capable of real-time, in-situ detection of key phytohormones—SA, IAA, MeJA, and ET—alongside nitrate, ammonium, and pH in both plant sap and soil. The sensor modules demonstrated high sensitivity, stability, and selectivity. Through extensive calibration and validation against standard chromatographic methods, the sensor suite proved highly reliable (Pearson $r > 0.98$), enabling continuous monitoring of both hormonal and nutrient dynamics under varying irrigation and N regimes. The deployment in bell pepper plants revealed distinct biochemical responses—reduced nitrate uptake and elevated hormonal accumulation under water stress—confirming the sensor's ability to capture complex physiological signaling and nutrient crosstalk in real time. The integration of hormonal and N sensing within a single platform provides a novel tool to decode endogenous plant signaling networks governing stress adaptation and nutrient assimilation. Furthermore, the ability to concurrently measure soil and plant N levels allows real-time feedback control for efficient fertilizer application, minimizing N losses and improving environmental sustainability. Integration

of these high-resolution sensor data with an LSTM prediction model provided predictive capability beyond real-time sensing. The LSTM model effectively captured temporal dependencies in plant nutrient and hormonal fluctuations, achieving R^2 values between 0.69 and 0.86 and low RMSE values (< 0.5 ppm for nitrate/ammonium and < 0.4 μM for hormones). This synergy between precision sensing and machine learning represents a powerful framework for proactive decision-making in precision agriculture, where nutrient management and stress mitigation can be optimized through data-driven predictions. Future studies should expand upon this foundation by integrating larger, more diverse datasets into the LSTM training process to enhance generalization across different crop species, soil types, and climatic conditions. A broader dataset would allow the model to learn more robust patterns of nutrient–hormone coupling and better anticipate stress-induced anomalies. Additionally, the inclusion of complementary environmental parameters (e.g., temperature, humidity, and light intensity) can improve prediction accuracy and contextual understanding. The future integration of wireless communication modules and cloud-based analytics could further extend this system's potential toward scalable, autonomous, and intelligent farm monitoring networks.

Research Funding

This work was supported in part by the National Science Foundation award no. 2138701 and in part by the Agriculture and Food Research Initiative, project award no. 2023-67021-40548, from the U.S. Department of Agriculture's National Institute of Food and Agriculture.

Author Contributions

N. I. Hossain contributed to sensor development and testing, data analysis, and manuscript drafting. M. Solaiman contributed to machine learning modeling, data analysis, and manuscript drafting. S. Tabassum conceptualized and supervised the entire project, reviewed and revised the manuscript, and was responsible for acquisition of funding for this project.

Competing Interests

The author(s) declare no competing interests.

Data Availability

The datasets generated during and/or analyzed during the current study are available from the corresponding author on reasonable request.

References

1. Lipper, L. *et al.* Climate-smart agriculture for food security. *Nature Clim Change* **4**, 1068–1072 (2014).
2. *World Agriculture towards 2030/2050: The 2012 Revision*. (2012). doi:10.22004/ag.econ.288998.
3. Gebbers, R. & Adamchuk, V. I. Precision Agriculture and Food Security. *Science* **327**, 828–831 (2010).
4. Babcock, B. A. The Effects of Uncertainty on Optimal Nitrogen Applications. *Review of Agricultural Economics* **14**, 271–280 (1992).
5. Grusak, M. A., Broadley, M. R. & White, P. J. Plant Macro- and Micronutrient Minerals. in *eLS* 1–6 (John Wiley & Sons, Ltd, 2016). doi:10.1002/9780470015902.a0001306.pub2.
6. Zhao, D., Reddy, K. R., Kakani, V. G. & Reddy, V. R. Nitrogen deficiency effects on plant growth, leaf photosynthesis, and hyperspectral reflectance properties of sorghum. *European Journal of Agronomy* **22**, 391–403 (2005).
7. Gloser, V. *et al.* Early Changes in Nitrate Uptake and Assimilation Under Drought in Relation to Transpiration. *Front. Plant Sci.* **11**, (2020).
8. Bista, D. R., Heckathorn, S. A., Jayawardena, D. M., Mishra, S. & Boldt, J. K. Effects of Drought on Nutrient Uptake and the Levels of Nutrient-Uptake Proteins in Roots of Drought-Sensitive and -Tolerant Grasses. *Plants (Basel)* **7**, 28 (2018).
9. Shah, A. N. *et al.* Nitrogen use efficiency in cotton: Challenges and opportunities against environmental constraints. *Frontiers in Plant Science* **13**, (2022).
10. Dybowski, D., Dzierzbicka-Glowacka, L. A., Pietrzak, S., Juszkowska, D. & Puszkarczuk, T. Estimation of nitrogen leaching load from agricultural fields in the Puck Commune with an interactive calculator. *PeerJ* **8**, e8899 (2020).

11. Wang, H. *et al.* Quantifying Phosphorus Leaching Loss from Mollisol with Organic Amendments. *Agronomy* **12**, 2490 (2022).
12. Rise in Greenhouse Gas Concentrations Jeopardizes Paris Agreement Temperature Targets | UNFCCC. https://unfccc.int/news/rise-in-greenhouse-gas-concentrations-jeopardizes-paris-agreement-temperature-targets.
13. Bellido-Pedraza, C. M. *et al.* Nitrous Oxide Emissions from Nitrite Are Highly Dependent on Nitrate Reductase in the Microalga Chlamydomonas reinhardtii. *International Journal of Molecular Sciences* **23**, 9412 (2022).
14. Stafford, J. V. Implementing Precision Agriculture in the 21st Century. *Journal of Agricultural Engineering Research* **76**, 267–275 (2000).
15. Zhang, N., Wang, M. & Wang, N. Precision agriculture—a worldwide overview. *Computers and Electronics in Agriculture* **36**, 113–132 (2002).
16. Vega, A., O'Brien, J. A. & Gutiérrez, R. A. Nitrate and hormonal signaling crosstalk for plant growth and development. *Current Opinion in Plant Biology* **52**, 155–163 (2019).
17. Liu, J. *et al.* Salicylic Acid, a Multifaceted Hormone, Combats Abiotic Stresses in Plants. *Life (Basel)* **12**, 886 (2022).
18. Pál, M., Janda, T. & Szalai, G. Abscisic Acid May Alter the Salicylic Acid-Related Abiotic Stress Response in Maize. *Journal of Agronomy and Crop Science* **197**, 368–377 (2011).
19. Sah, S. K., Reddy, K. R. & Li, J. Abscisic Acid and Abiotic Stress Tolerance in Crop Plants. *Front Plant Sci* **7**, 571 (2016).
20. Wang, J., Song, L., Gong, X., Xu, J. & Li, M. Functions of Jasmonic Acid in Plant Regulation and Response to Abiotic Stress. *Int J Mol Sci* **21**, 1446 (2020).

21. Krouk, G. *et al.* Nitrate-Regulated Auxin Transport by NRT1.1 Defines a Mechanism for Nutrient Sensing in Plants. *Developmental Cell* **18**, 927–937 (2010).
22. Liu, J. *et al.* Auxin transport in maize roots in response to localized nitrate supply. *Annals of Botany* **106**, 1019–1026 (2010).
23. Song, W. *et al.* Auxin distribution is differentially affected by nitrate in roots of two rice cultivars differing in responsiveness to nitrogen. *Annals of Botany* **112**, 1383–1393 (2013).
24. Xu, J. *et al.* The interaction between nitrogen availability and auxin, cytokinin, and strigolactone in the control of shoot branching in rice (Oryza sativa L.). *Plant Cell Rep* **34**, 1647–1662 (2015).
25. Ma, W. *et al.* Auxin biosynthetic gene 2 is involved in low nitrogen-mediated reprogramming of root architecture in Arabidopsis. *The Plant Journal* **78**, 70–79 (2014).
26. Tian, Q.-Y., Sun, P. & Zhang, W.-H. Ethylene is involved in nitrate-dependent root growth and branching in Arabidopsis thaliana. *New Phytologist* **184**, 918–931 (2009).
27. Zheng, D. *et al.* The nitrate transporter NRT2.1 functions in the ethylene response to nitrate deficiency in rabidopsis. *Plant, Cell & Environment* **36**, 1328–1337 (2013).
28. Cheng, W., Zhang, A., Zhu, J., Li, Y. & Wang, P. Study of Salicylic Acid Influence on Seedling Growth and Nitrogen Metabolism in Watermelon (Citrullus lanatus L.). *Journal of Food Engineering and Technology* **7**, 47–47 (2018).
29. Hou, S. & Tsuda, K. Salicylic acid and jasmonic acid crosstalk in plant immunity. *Essays Biochem* **66**, 647–656 (2022).
30. Zhang, G.-B., Yi, H.-Y. & Gong, J.-M. The Arabidopsis Ethylene/Jasmonic Acid-NRT Signaling Module Coordinates Nitrate Reallocation and the Trade-Off between Growth and Environmental Adaptation[W][OPEN]. *Plant Cell* **26**, 3984–3998 (2014).

31. Wu, X. *et al.* The roles of jasmonate signalling in nitrogen uptake and allocation in rice (Oryza sativa L.). *Plant, Cell & Environment* **42**, 659–672 (2019).
32. Khan, M. I. R. *et al.* Role of ethylene in responses of plants to nitrogen availability. *Front. Plant Sci.* **6**, (2015).
33. Etesami, H. & Glick, B. R. Bacterial indole-3-acetic acid: A key regulator for plant growth, plant-microbe interactions, and agricultural adaptive resilience. *Microbiological Research* **281**, 127602 (2024).
34. Pu, W., Wang, W., Du, R., Xie, D. & Shan, X. Reciprocal regulation of nitrate and jasmonate signaling by JASMONATE ZIM DOMAIN PROTEIN 1 coordinates plant growth and defense. *New Phytologist* **n/a**,.
35. O'Brien, J. A. *et al.* Nitrate Transport, Sensing, and Responses in Plants. *Molecular Plant* **9**, 837–856 (2016).
36. Salinas, P., Velozo, S. & Herrera-Vásquez, A. Salicylic acid accumulation: emerging molecular players and novel perspectives on plant development and nutrition. *J Exp Bot* **76**, 1950–1969 (2025).
37. Fu, Y.-F., Yang, X.-Y., Zhang, Z.-W. & Yuan, S. Synergistic effects of nitrogen metabolites on auxin regulating plant growth and development. *Front. Plant Sci.* **13**, (2022).
38. Feng, J. & Barker, A. V. Ethylene evolution and ammonium accumulation by nutrient-stressed tomato plants. *Journal of Plant Nutrition* **15**, 137–153 (1992).
39. Kim, J. Y., Song, J. T. & Seo, H. S. Ammonium-mediated reduction in salicylic acid content and recovery of plant growth in Arabidopsis siz1 mutants is modulated by NDR1 and NPR1. *Plant Signaling & Behavior* **16**, 1928819 (2021).

40. Pandey, A. *et al.* Jasmonate signaling modulates root growth by suppressing iron accumulation during ammonium stress. *Plant Physiol* **196**, 2213–2231 (2024).
41. Li, G. *et al.* Ammonium-induced shoot ethylene production is associated with the inhibition of lateral root formation in Arabidopsis. *J Exp Bot* **64**, 1413–1425 (2013).
42. Zhou, T., Zhang, L., Wu, P., Feng, Y. & Hua, Y. Salicylic Acid Is Involved in the Growth Inhibition Caused by Excessive Ammonium in Oilseed Rape (Brassica napus L.). *J. Agric. Food Chem.* **72**, 14419–14432 (2024).
43. Hood-Nowotny, R., Umana, N. H.-N., Inselbacher, E., Oswald- Lachouani, P. & Wanek, W. Alternative Methods for Measuring Inorganic, Organic, and Total Dissolved Nitrogen in Soil. *Soil Science Society of America Journal* **74**, 1018–1027 (2010).
44. Daniel, A., Birot, D., Lehaitre, M. & Poncin, J. Characterization and reduction of interferences in flow-injection analysis for the in situ determination of nitrate and nitrite in sea water. *Analytica Chimica Acta* **308**, 413–424 (1995).
45. Schroeder, D. C. The analysis of nitrate in environmental samples by reversed-phase HPLC. *J Chromatogr Sci* **25**, 405–408 (1987).
46. Yoshizumi, Kunio., Aoki, Kazuyuki., Matsuoka, Toshikazu. & Asakura, Shukuji. Determination of nitrate by a flow system with a chemiluminescent nitrogen oxide (NOx) analyzer. *Anal. Chem.* **57**, 737–740 (1985).
47. Englmaier, P. Nitrate analysis by gas-liquid chromatography using the nitration of 2,4-dimethylphenol in sulphuric acid. *Journal of Chromatography A* **270**, 243–251 (1983).
48. Salem, M. A., Wang, J. Y. & Al-Babili, S. Metabolomics of plant root exudates: From sample preparation to data analysis. *Front. Plant Sci.* **13**, (2022).

49. Dalal, R. C. & Henry, R. J. Simultaneous Determination of Moisture, Organic Carbon, and Total Nitrogen by Near Infrared Reflectance Spectrophotometry. *Soil Science Society of America Journal* **50**, 120–123 (1986).
50. Loaiza Puerta, V., Six, J., Wittwer, R., van der Heijden, M. & Pujol Pereira, E. I. Comparable bacterial-mediated nitrogen supply and losses under organic reduced tillage and conventional intensive tillage. *European Journal of Soil Biology* **95**, 103121 (2019).
51. Cunningham, L. & Freiser, H. Coated-wire ion-selective electrodes. *Analytica Chimica Acta* **180**, 271–279 (1986).
52. Bobacka, J., Ivaska, A. & Lewenstam, A. Potentiometric Ion Sensors. *Chem. Rev.* **108**, 329–351 (2008).
53. Silvester, D. S. Recent advances in the use of ionic liquids for electrochemical sensing. *Analyst* **136**, 4871–4882 (2011).
54. Hu, J., Stein, A. & Bühlmann, P. Rational design of all-solid-state ion-selective electrodes and reference electrodes. *TrAC Trends in Analytical Chemistry* **76**, 102–114 (2016).
55. Gao, W. *et al.* Fully integrated wearable sensor arrays for multiplexed in situ perspiration analysis. *Nature* **529**, 509–514 (2016).
56. Anastasova-Ivanova, S. *et al.* Development of miniature all-solid-state potentiometric sensing system. *Sensors and Actuators B: Chemical* **146**, 199–205 (2010).
57. Inam, A. K. M. S. *et al.* Circular Sensing of Nitrate Levels in Water With Flexible Screen-Printed Sensors on Biodegradable Cellulose Substrate. *IEEE Sensors Letters* **7**, 1–4 (2023).
58. Garland, N. T. *et al.* Flexible Laser-Induced Graphene for Nitrogen Sensing in Soil. *ACS Appl. Mater. Interfaces* **10**, 39124–39133 (2018).

59. Dam, V. A. T., Zevenbergen, M. A. G. & van Schaijk, R. Toward wearable patch for sweat analysis. *Sensors and Actuators B: Chemical* **236**, 834–838 (2016).
60. Pereira, A. N. *et al.* Flexible Sensor Suite Integrated Into Textile for Calcium Ion and Fall Detection. *IEEE Sensors Letters* **6**, 1–4 (2022).
61. Inam, A. K. M. S. *et al.* Integrated sensor platform for real-time monitoring of nitrate, ammonium, temperature, and pH in aquatic environments. *Talanta* **296**, 128466 (2026).
62. Athavale, R. *et al.* Robust Solid-Contact Ion Selective Electrodes for High-Resolution In Situ Measurements in Fresh Water Systems. *Environ. Sci. Technol. Lett.* **4**, 286–291 (2017).
63. Yuan, D. *et al.* All-Solid-State Potentiometric Sensors with a Multiwalled Carbon Nanotube Inner Transducing Layer for Anion Detection in Environmental Samples. *Anal. Chem.* **87**, 8640–8645 (2015).
64. Lai, C.-Z., Fierke, M. A., Stein, A. & Bühlmann, P. Ion-Selective Electrodes with Three-Dimensionally Ordered Macroporous Carbon as the Solid Contact. *Anal. Chem.* **79**, 4621–4626 (2007).
65. Zhu, J., Li, X., Qin, Y. & Zhang, Y. Single-piece solid-contact ion-selective electrodes with polymer–carbon nanotube composites. *Sensors and Actuators B: Chemical* **148**, 166–172 (2010).
66. Lindfors, T. & Ivaska, A. Stability of the Inner Polyaniline Solid Contact Layer in All-Solid-State K+-Selective Electrodes Based on Plasticized Poly(vinyl chloride). *Anal. Chem.* **76**, 4387–4394 (2004).
67. Guzinski, M. *et al.* PEDOT(PSS) as Solid Contact for Ion-Selective Electrodes: The Influence of the PEDOT(PSS) Film Thickness on the Equilibration Times. *Anal. Chem.* **89**, 3508–3516 (2017).

68. Riam, S. Z. *et al.* AQUA-FINS: Advanced Quantitative Underwater Analysis by a Flexible Integrated Nitrate Sensor. *Advanced Sensor Research* **4**, 2500010 (2025).
69. Bobacka, J. Potential Stability of All-Solid-State Ion-Selective Electrodes Using Conducting Polymers as Ion-to-Electron Transducers. *Anal. Chem.* **71**, 4932–4937 (1999).
70. Cuartero, M., Colozza, N., Fernández-Pérez, B. M. & Crespo, G. A. Why ammonium detection is particularly challenging but insightful with ionophore-based potentiometric sensors – an overview of the progress in the last 20 years. *Analyst* **145**, 3188–3210 (2020).
71. Fayose, T. *et al.* Concurrent measurement of nitrate and ammonium in water and soil samples using ion-selective electrodes: Tackling sensitivity and precision issues. *Analytical Science Advances* **2**, 279–288 (2021).
72. Benco, J. S., Nienaber, H. A. & McGimpsey, W. G. Synthesis of an ammonium ionophore and its application in a planar ion-selective electrode. *Anal Chem* **75**, 152–156 (2003).
73. Joon, N. K., He, N., Ruzgas, T., Bobacka, J. & Lisak, G. PVC-Based Ion-Selective Electrodes with a Silicone Rubber Outer Coating with Improved Analytical Performance. *Anal. Chem.* **91**, 10524–10531 (2019).
74. Gan, T., Hu, C., Chen, Z. & Hu, S. Fabrication and application of a novel plant hormone sensor for the determination of methyl jasmonate based on self-assembling of phosphotungstic acid–graphene oxide nanohybrid on graphite electrode. *Sensors and Actuators B: Chemical* **151**, 8–14 (2010).
75. Wang, Z. *et al.* Au@SnO2-vertical graphene-based microneedle sensor for in-situ determination of abscisic acid in plants. *Materials Science and Engineering: C* **127**, 112237 (2021).

76. Gan, T., Hu, C., Chen, Z. & Hu, S. A disposable electrochemical sensor for the determination of indole-3-acetic acid based on poly(safranine T)-reduced graphene oxide nanocomposite. *Talanta* **85**, 310–316 (2011).
77. Hu, Y. *et al.* A multifunctional ratiometric electrochemical sensor for combined determination of indole-3-acetic acid and salicylic acid. *RSC Adv.* **10**, 3115–3121 (2020).
78. Hossain, N. I., Noushin, T. & Tabassum, S. Leaf-FIT: A Wearable Leaf Sensor for In-Situ and Real-Time Monitoring of Plant Phytohormones. in *2021 IEEE Sensors* 1–4 (2021). doi:10.1109/SENSORS47087.2021.9639842.
79. Hossain, N. I. & Tabassum, S. Fruit-FIT: Drone Interfaced Multiplexed Sensor Suite to Determine the Fruit Ripeness. in *2022 IEEE Sensors* 1–4 (2022). doi:10.1109/SENSORS52175.2022.9967097.
80. Ishtiaque Hossain, N. & Tabassum, S. Stem-FIT: a Microneedle-based Multi-parametric Sensor for In Situ Monitoring of Salicylic Acid and pH Levels in Live Plants. in *2022 IEEE 17th International Conference on Nano/Micro Engineered and Molecular Systems (NEMS)* 312–316 (2022). doi:10.1109/NEMS54180.2022.9791212.
81. Hossain, N. I. & Tabassum, S. Leaf-mounted microneedle-based multisensory platform for multiplexed monitoring of phytohormones in live plants. *in Proc. Hilton Head 2022: A Solid-State Sensors, Actuators and Microsystems* (2022).
82. Hossain, N. I. & Tabassum, S. A hybrid multifunctional physicochemical sensor suite for continuous monitoring of crop health. *Sci Rep* **13**, 9848 (2023).
83. Hossain, N. I., Noushin, T. & Tabassum, S. Tattoo-like Flexible Ethylene Sensor for Plant Stress Monitoring in Real-time. *IEEE Sensors Journal* 1–1 (2023) doi:10.1109/JSEN.2023.3327547.

84. Viscarra Rossel, R. A. & Bouma, J. Soil sensing: A new paradigm for agriculture. *Agricultural Systems* **148**, 71–74 (2016).

85. *Food Analysis*. (Springer US, Boston, MA, 2010). doi:10.1007/978-1-4419-1478-1.

86. Solaiman, M., Galib, A. R., Riam, S. Z., Sarwar Inam, A. & Tabassum, S. Real-time potentiometric sensing of soil nitrate: Depth-resolved monitoring across plant species with varying root structures. *Computers and Electronics in Agriculture* **239**, 110929 (2025).

87. Sangmen, E. D. *et al.* Flexible Biodegradable Leaf-Wearable Sensor for Monitoring Stress-Induced Methanol Emission from Plants. *in the Proceedings of Hilton Head Workshop: A Solid-State Sensors, Actuators and Microsystems Workshop* (2024).

88. Sangmen, E. D. *et al.* Sensors for In-situ Monitoring of Methanol and Terpene Gas Emissions from Nitrogen-Stressed Cotton Plants Throughout Their Lifecycle. in (New Orleans, LA, 2025).

89. Kundu, S., Tabassum, S. & Kumar, R. Plasmonic Point-of-Care Device for Sepsis Biomarker Detection. *IEEE Sensors Journal* **21**, 18837–18846 (2021).

90. Smil, V. Nitrogen in crop production: An account of global flows. *Global Biogeochemical Cycles* **13**, 647–662 (1999).

91. Riemann, M. *et al.* Exploring Jasmonates in the Hormonal Network of Drought and Salinity Responses. *Front Plant Sci* **6**, 1077 (2015).

92. Wang, J., Song, L., Gong, X., Xu, J. & Li, M. Functions of Jasmonic Acid in Plant Regulation and Response to Abiotic Stress. *Int J Mol Sci* **21**, 1446 (2020).

93. Kim, Y.-H. *et al.* Comparative analysis of endogenous hormones level in two soybean (Glycine max L.) lines differing in waterlogging tolerance. *Front Plant Sci* **6**, 714 (2015).

94. Lastochkina, O. *et al.* Role of Endogenous Salicylic Acid as a Hormonal Intermediate in the Bacterial Endophyte Bacillus subtilis-Induced Protection of Wheat Genotypes Contrasting in Drought Susceptibility under Dehydration. *Plants (Basel)* **11**, 3365 (2022).
95. Llanes, A., Andrade, A., Alemano, S. & Luna, V. Alterations of Endogenous Hormonal Levels in Plants under Drought and Salinity. *American Journal of Plant Sciences* **07**, 1357 (2016).
96. Goyal, S. S. & Huffaker, R. C. Nitrogen Toxicity in Plants. in *Nitrogen in Crop Production* 97–118 (John Wiley & Sons, Ltd, 1984). doi:10.2134/1990.nitrogenincropproduction.c6.

Supplementary Files

This is a list of supplementary files associated with this preprint. Click to download.

- IonpaperSupplementaryupdate10212025.docx